CONDENSED MATTER PHYSICS

Discovery of log-periodic oscillations in ultraquantum topological materials

Huichao Wang[1,2,3]*, Haiwen Liu[4]*, Yanan Li[1,2], Yongjie Liu[5], Junfeng Wang[5], Jun Liu[6], Ji-Yan Dai[3], Yong Wang[6], Liang Li[5], Jiaqiang Yan[7], David Mandrus[7,8], X. C. Xie[1,2,9†], Jian Wang[1,2,9†]

Quantum oscillations are usually the manifestation of the underlying physical nature in condensed matter systems. Here, we report a new type of log-periodic quantum oscillations in ultraquantum three-dimensional topological materials. Beyond the quantum limit (QL), we observe the log-periodic oscillations involving up to five oscillating cycles (five peaks and five dips) on the magnetoresistance of high-quality single-crystal $ZrTe_5$, virtually showing the clearest feature of discrete scale invariance (DSI). Further, theoretical analyses show that the two-body quasi-bound states can be responsible for the DSI feature. Our work provides a new perspective on the ground state of topological materials beyond the QL.

INTRODUCTION

The discrete scale invariance (DSI) feature originates from the log-periodic corrections to scaling, and consequently, observables are scale invariant only for certain geometrical scaling factors, reminiscent of fractal systems (*1*). In a scale-invariant system, the quantization effect can spontaneously break the continuous scale invariance down to DSI, which is a theoretically identified issue in quantum physics (*2*) but with rare manifestation in experiments. Governed by the Efimov equation, the DSI emerges as a distinctive feature of Efimov trimer bound states (*3*–*5*), which have been observed in cold atom experiments (*6*–*10*). The exotic scaling law and mathematical description of the Efimov effect can be further shared by the Efimov-like or Efimovian phenomena (*11*). In condensed matter physics, the DSI has been theoretically proposed to appear in quasi-bound states of massless Dirac fermions in the atomic collapse under supercritical Coulomb attraction (*12*–*14*). However, experimental evidence for the clear demonstration of the DSI has not been presented. The recently studied Dirac system with two types of carriers can satisfy the supercritical collapse condition for the appearance of DSI, providing a promising platform to search for this rare and important phenomenon in quantum physics. Moreover, the potential link between the supercritical atomic collapse in topological systems and the appearance of DSI feature is also of particular interest.

In condensed matter physics, quantum oscillation revealed by magnetotransport investigation has been a powerful experimental technique to detect the underlying physics of solid-state systems. In the presence of a magnetic field (B), the Shubnikov–de Haas (SdH) oscillations showing a periodicity in $1/B$ can be usually observed at low temperatures and high magnetic fields for a clean single-crystalline material (*15*). As a paradigm of Landau quantization of the energy levels, the SdH effect provides insights toward mapping the Fermi surface (*16*). Besides, in ring or cylinder structures, the Aharonov-Bohm (AB) and Altshuler-Aronov-Spivak (AAS) effects can also induce quantum oscillations in magnetoresistance (MR), where the oscillations are periodic in B. The observation of these effects offers an illustration of the quasiparticle quantum interference in mesoscopic systems (*17*). Thus, it would be interesting to explore the DSI behavior by magnetotransport measurements.

In this work, we report a new type of log-periodic quantum oscillations that is demonstrated by the systematical magnetotransport results from different samples and different facilities with the maximum magnetic field up to 58 T. For the underlying physics, we find that it cannot be understood in the scenarios of conventional quantum oscillations such as the SdH effect (even considering the Zeeman splitting) or other previously known mechanisms beyond the quantum limit (QL). On the other hand, the log periodicity of the structures in the MR is reminiscent of the DSI behavior, which indicates that the system has a geometric series of length scales. Further, theoretical derivations show that the Dirac fermions with supercritical Coulomb attraction can give rise to the two-body quasi-bound states with DSI feature. Our work provides a new perspective on the ground state of topological materials beyond the QL. The discovery of a new type of quantum oscillation with the log$B$ periodicity represents a new phenomenon beyond the Landau level physics; to our knowledge, this is the first time that DSI has been detected by magnetotransport measurements in condensed matter systems. Our work also indicates that the intriguing log-periodic oscillations are potentially universal in the topological materials with Coulomb attraction, which opens up a new direction to explore the DSI behavior and the atomic collapse phenomenon.

RESULTS

Crystal characterizations

$ZrTe_5$ crystallizes in a layered orthorhombic structure with the space group *Cmcm* (*18*). Along the *a* axis, Zr and Te atoms are bonded as trigonal prismatic chains of "$ZrTe_3$," which are linked along the *c* axis via parallel zigzag chains of "Te_2." This forms one layer of $ZrTe_5$ in the *ac* plane, and individual layers are coupled via van der Waals interactions along the *b* axis. The $ZrTe_5$ material was ever intensively investigated for the resistivity peak at certain temperatures, and its SdH

[1]International Center for Quantum Materials, School of Physics, Peking University, Beijing 100871, China. [2]Collaborative Innovation Center of Quantum Matter, Beijing 100871, China. [3]Department of Applied Physics, The Hong Kong Polytechnic University, Kowloon, Hong Kong, China. [4]Center for Advanced Quantum Studies, Department of Physics, Beijing Normal University, Beijing 100875, China. [5]Wuhan National High Magnetic Field Center, Huazhong University of Science and Technology, Wuhan 430074, China. [6]Center of Electron Microscopy, State Key Laboratory of Silicon Materials, School of Materials Science and Engineering, Zhejiang University, Hangzhou 310027, China. [7]Materials Science and Technology Division, Oak Ridge National Laboratory, Oak Ridge, TN 37831, USA. [8]Department of Materials Science and Engineering, University of Tennessee, Knoxville, TN 37996, USA. [9]CAS Center for Excellence in Topological Quantum Computation, University of Chinese Academy of Sciences, Beijing 100190, China.
*These authors contributed equally to this work.
†Corresponding author. Email: jianwangphysics@pku.edu.cn (J.W.); xcxie@pku.edu.cn (X.C.X)

oscillations were reported to reveal the very tiny and anisotropic Fermi surface (*18*–*20*). Recently, the theoretical prediction of topologically nontrivial nature of the material has triggered a new wave of research boom (*21*). On the basis of the recent reports on the system from both theorists and experimentalists (*22*–*35*), it is known that the system is extremely sensitive to the cell volume, and thus, the measured physical properties of $ZrTe_5$ are divergent in different samples modified by the growth condition (table S1).

$ZrTe_5$ single crystals used in this work were grown out of the Te-flux method (*36*). The samples were well characterized by measuring x-ray single-crystal diffraction, elemental analysis, electrical resistivity, and thermopower, confirming that our crystals are stoichiometric (*22*). Our energy-dispersive spectroscopy results reveal an atomic ratio of the samples with Zr:Te ≈ 1:5 (table S2). We also used an FEI Titan Cs-corrected cross-sectional scanning transmission electron microscope (STEM) operating at 200 kV to further examine the crystalline nature of the $ZrTe_5$ sample. Figure 1A shows the atomic layer-by-layer high-angle annular dark-field (HAADF) STEM image of a typical $ZrTe_5$ sample, which demonstrates the high-quality nature. The deduced lattice constants of a = 0.398 nm and b = 1.450 nm (Fig. 1A, inset) are consistent with previous reports (*21*–*23*).

Temperature dependence of resistivity and Hall traces

Figure 1B shows typical resistivity versus temperature (*RT*) behavior of the $ZrTe_5$ crystals [sample 1 (s1) and s6]. A crossover can be observed in the *RT* curves from metallic behavior above 200 K to a semiconducting-like upturn with saturation at low temperatures. The samples from the same batch show similar properties. The *RT* characteristic differs from those in most of the previous literature in which the $ZrTe_5$ usually shows a sample-dependent resistance peak at 60 to 150 K. On the other hand, a similar *RT* behavior of $ZrTe_5$ is also observed and reported by other research groups (*22*, *32*), and the absence of the resistance peak is attributed to the much smaller density of impurities and defects in the samples. This proposal appears to be consistent with our results because the Te deficiency can be largely reduced in our samples by using the self–Te-flux method and further modifying the growth parameters (*22*).

Figure 1C shows the measured Hall traces obtained on s1. At 2 K, the Hall coefficient shows a positive slope at low field (<1.5 T) and then turns negative in the high-field regime (>1.5 T), indicating the coexistence of both hole carriers and electron carriers in the $ZrTe_5$ crystals (*24*, *25*). On the basis of the previous literature (*22*–*34*), the Hall behavior in $ZrTe_5$ shows dissimilarities in different samples, and the carriers at low temperatures are reported to be holes, electrons, or both types. For the samples with a resistance peak in the *RT* behavior, it is reported that the carriers change from dominated electrons at lower temperature to dominated holes at higher temperatures (*29*). The sign change of Hall at the temperature where the peak appears is attributed to a proposal of Lifshitz transition. However, this would not happen in the samples without showing a resistance peak (*22*, *32*). The differences of the carriers in these two classes of $ZrTe_5$ samples are compared and clarified recently (*22*). Our Hall results are consistent with those of the samples without a resistance peak (*22*, *32*). Besides, most previous reports show the existence of hole carriers at low temperatures in $ZrTe_5$ crystals (*22*, *24*, *25*, *34*), which also support our observation in Hall measurements.

According to the analysis of measured magnetoresistivity and Hall resistivity, we obtain the conductivity tensors σ_{xx} and σ_{xy} (fig. S1). In a two-carrier model analysis of the σ_{xx} and σ_{xy} (*37*), the carrier density and mobility of our sample at selected temperatures are estimated and shown in Fig. 1D. The results indicate that the hole carriers have a quite low density of 2.6×10^{15} cm^{-3} and a high mobility of about 3.9×10^5 cm^2 V^{-1} s^{-1} at 2 K (*25*, *29*), while the electrons show a higher density of 2.4×10^{16} cm^{-3} with a lower mobility of 2900 cm^2 V^{-1} s^{-1}. In the $ZrTe_5$ system with very low carrier densities, the QL can be reached under a very small magnetic field (*31*). The estimated QL for our samples is about 0.2 T (see Materials and methods), which offers an exciting playground to explore new physics in the ultraquantum regime.

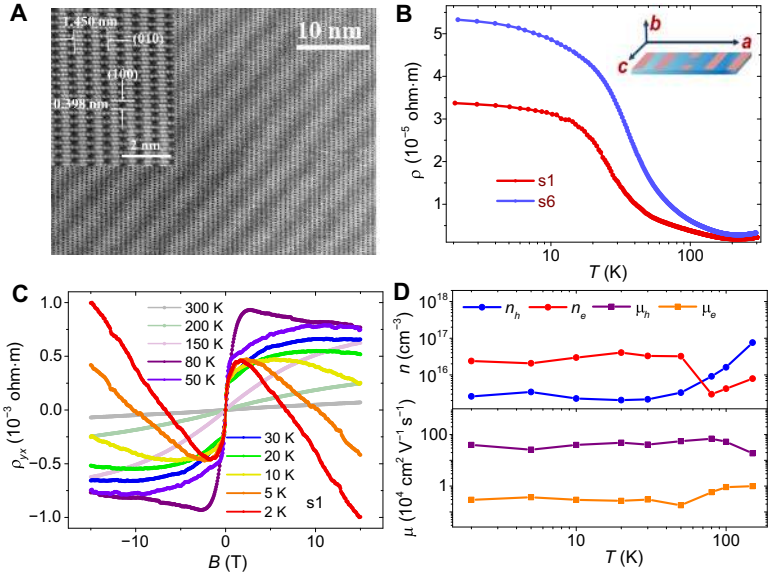

Fig. 1. Characterization of high-quality $ZrTe_5$ crystal. (**A**) HAADF STEM image of a typical $ZrTe_5$ sample. The inset shows the atomic resolution. (**B**) *RT* characteristic of $ZrTe_5$. Inset shows the schematic for electrical transport measurements. (**C**) Hall traces of s1 versus *B* at selected temperatures from 2 to 300 K. (**D**) Temperature dependence of the estimated mobility and carrier density of the carriers in $ZrTe_5$ by analyzing the Hall data with a two-carrier model.

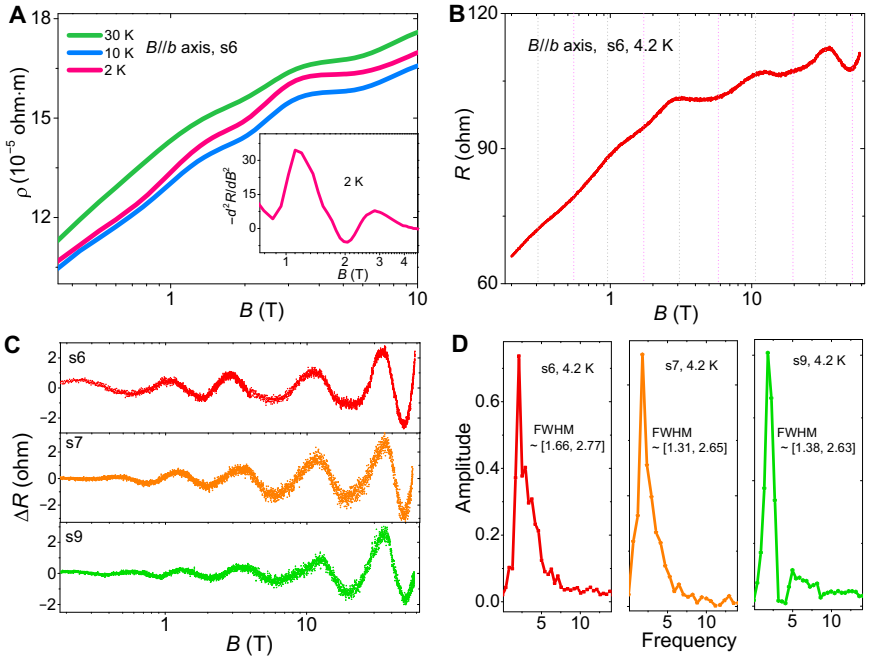

Fig. 2. Log-periodic MR oscillations in $ZrTe_5$. (**A**) Resistivity of s6 versus B at low temperatures in a static perpendicular magnetic field. The inset shows the second derivative result of MR data at 2 K. (**B**) MR behavior of s6 in an ultrahigh magnetic field up to 58 T at 4.2 K. Dotted lines serve as guides to the eye. (**C**) Extracted MR oscillations in $ZrTe_5$ samples (s6, s7, and s9) at 4.2 K. (**D**) FFT results for the log-periodic oscillation data in the form of ΔR versus $\log(B/B')$ with $B' = 1$ T.

Log-periodic MR oscillations

Figure 2A shows the longitudinal MR behavior of s6 at low temperatures in a perpendicular magnetic field ($B//b$ axis). We select the resistance at 5 T for a comparison of the MR results in different literature. In our samples, the $R(5\ T)/R(0\ T)$ varies from 3 to 8, which is on the same order of magnitude as that found in most previous publications (*22*, *23*, *30*, *33*, *34*). Previous studies reported that the value of $R(5\ T)/R(0\ T)$ at around 2 K can vary from 1.2 to 235, and that the shapes of the reported MR curves also very for different $ZrTe_5$ samples (all with $B//b$ axis) (*22*–*34*).

In a semilogarithmic scale, we observe MR oscillations that are superimposed on a large MR background. By computing the second derivative of the raw MR data at 2 K, the oscillations can be seen more clearly, as shown in the inset of Fig. 2A. Two peaks at ~1.1 and ~2.9 T are obvious. We further perform extended measurements in an ultrahigh magnetic field up to 58 T. At 4.2 K, we also observe distinct MR oscillations in the small magnetic field regime, and more oscillations appear above 3 T (Fig. 2B). To guide the eye, dotted lines mark all the observable MR extrema. The approximate equidistance of lines indicates that the oscillations are virtually periodic in the logarithmic magnetic field. The log-periodic law is more distinctly revealed after a background subtraction (see Materials and methods and fig. S2). As shown in Fig. 2C, the novel oscillations are reproducible in different $ZrTe_5$ samples (s6, s7, and s9; see fig. S3, s2 and s10). In the fast Fourier transform (FFT) analysis of the oscillation data [ΔR versus $\log(B/B')$], the sharp frequency (F) peak at $F \approx 2$ confirms the log$B$ period. Here, we use $B' = 1$ T to realize a dimensionless transformation and respectively label the full width at half maximum (FWHM) of the peak in Fig. 2D.

As the temperature is increased, the log-periodic oscillations become weaker and gradually disappear one after the other (Fig. 3A). Nevertheless, it is unexpected that the oscillations above 10 T could still survive at temperatures as high as 100 K (Fig. 3B). Figure 3C shows the temperature dependence of the log-periodic oscillations more clearly. We observe five oscillating cycles at 4.2 K, while only two cycles in large magnetic fields remain visible when the temperature is increased to 100 K and the oscillation feature is gone at 150 K. The FFT results at the selected temperatures further reveal that the oscillations maintain the same log period with the increasing temperature but disappear at 150 K (Fig. 3D).

We index the observed MR peak with an integer (n) and dip with a half ($n - 0.5$), and the corresponding magnetic field is signed as B_n. Figure 4A shows the index plot for the oscillations at 4.2 K. The behavior of $1/B_n$ versus n largely deviates the linear dependence (Fig. 4A, I to III), which is apparently different with the SdH effect even considering Zeeman splitting (see more details in the supplementary materials). The linear dependence in the plot of B_n versus n is also absent (fig. S4). In a semilogarithmic scale (Fig. 4, IV to VI), the linear dependence of $\log(B_n)$ on n further confirms the log-periodic property of the observed oscillations. In condensed matter systems, previously known quantum oscillations are mainly associated with either the Landau level physics (*16*), which is periodic in $1/B$, or the quantum interference effect (*17*), which is periodic in B. Our discovery of the log$B$ periodicity appreciably reveals a new class of quantum oscillations in condensed matter physics.

DISCUSSION AND THEORETICAL EXPLANATION

The log-periodic structures in the MR data are reminiscent of the DSI behavior, which indicates that the system has a geometric series of length scales (*1*). On the basis of the Hall data (Fig. 1C), the high mobility hole is from the Dirac band with linear dispersion (*25*, *29*). Since the carriers are very dilute, the system can be simplified into a two-body problem. The charge impurity or electron from trivial band

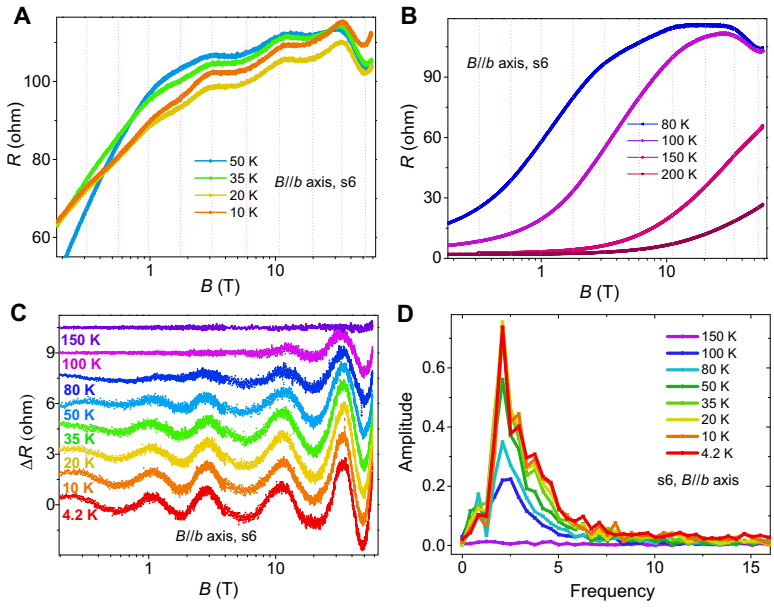

Fig. 3. Log-periodic MR oscillations at different temperatures. (**A**) MR behavior of s6 at relatively low temperatures. (**B**) MR behavior of s6 at relatively high temperatures. (**C**) MR oscillations in s6 after subtracting a smooth background from the raw data. Dotted lines serve as guides to the eye. (**D**) FFT results for the MR oscillations at different temperatures in the form of ΔR versus $\log(B/B')$ with $B' = 1$ T.

can act as a charge center to massless hole and give rise to a long-range Coulomb attraction $V(\vec{R}) = \frac{-e^2}{4\pi\varepsilon_0 R}$, with R denoting the distance (Fig. 4B). Because all terms are of the order R^{-1}, the massless Dirac Hamiltonian with Coulomb attraction remarkably obeys the scale invariance. After eliminating the angular wave function, the radial equation of each spinor element can be obtained, which is close to the Efimov equation (see more details in the supplementary materials): $-\frac{d^2}{dR^2}u(R) + \frac{\kappa^2}{R^2}u(R) - \left(\frac{E}{\hbar v_F} + \frac{\alpha}{R}\right)^2 u(R) = 0$. Here, E is the energy, $\alpha = \frac{e^2}{4\pi\varepsilon_0\hbar v_F}$ is the fine structure constant, $u(R)$ denotes the radial part of the spinor eigenfunction, and $\kappa = \pm1, \pm2\ldots$ denotes the angular momentum index (*12*). The supercritical Coulomb attraction with $\alpha > |\kappa|$ (supercritical collapse condition) guarantees the formation of quasi-bound states (*12*–*14*), while for subcritical case $\alpha < |\kappa|$, the states are absent. In the following, we focus on the lowest angular momentum channel with $\kappa = \pm1$. Thus, the radial momentum satisfies the formula $p_R^2 = \hbar^2\left[\left(\frac{E}{\hbar v_F} + \frac{\alpha}{R}\right)^2 - \frac{1}{R^2}\right]$. The semiclassical quantization $\int_{R_0}^{R_n} p\cdot dr = n\pi\hbar$ results in the DSI for the radius of the quasi-bound states $\frac{R_{n+1}}{R_n} = e^{\pi/s_0}$ with $s_0 = \sqrt{\alpha^2 - 1}$. The magnetic field introduces a new length scale $l_B = \sqrt{\hbar c/eB}$ and breaks the DSI of the quasi-bound states down to approximate DSI. The effect of magnetic field can be quantitatively analyzed by comparing the Landau level spacing $E_B = \sqrt{2}\hbar v_F/l_B$ with the Coulomb attraction $V(R_n) = \alpha\hbar v_F/R_n$, where R_n indicates the most probable radius of the nth quasi-bound states (see more details in the supplementary materials). Under the magnetic fields with $E_B < V(R_n)$, the system still has approximate spherical symmetry. However, the magnetic field generates a repulsive interaction that breaks the large-size states with $R_n > \sqrt{2s_0}l_B$, when E_B exceeds the Coulomb attraction energy. When the magnetic field is enlarged, the energy of the nth quasi-bound states approaches the Fermi energy at the magnetic field B_n. Figure 4C shows the numerical simulation of the spectrum under the magnetic field in which E_0 and L_0 denote the cutoff energy scale and the cutoff length scale, respectively. $|E_n|$ denotes the binding energy of the two-body quasi-bound states without any magnetic field, and B_n denotes the magnetic field value for the appearance of the nth quasi-bound states around the Fermi energy (Fig. 4C). The resonant scattering process between the mobile carriers and the two-body quasi-bound states influences the transport property at the Fermi level, which leads to a log-periodic correction to the MR.

On the basis of T-matrix approximation, we obtain the log-periodic oscillating component of the MR: $\Delta\rho_{xx} = \frac{\rho_0\sqrt{B[T]}\eta^2}{\sin^2\left(\frac{s_0}{2}\ln\left(\frac{B}{B_0}\right)\right) + \eta^2} - c\rho_0\sqrt{B[T]}$ (see details in the supplementary materials). Here, the first term denotes the log-periodic oscillations, and the second term indicates the background subtraction. The detailed derivation of the fitting formulas and more discussions on the Zeeman effect are given in the supplementary materials. Using this formula, we quantitatively reproduce the observed log-periodic oscillations in different samples s6, s7, and s9 at 4.2 K (black curves), as shown in Fig. 4D. On the basis of the fits, we obtain an averaging value of $s_0 \approx 5.4$ (see details in the supplementary materials), and thus, the Fermi velocity $v_F \approx 4.0 \times 10^5$ m/s can be deduced for the Dirac bands in $ZrTe_5$, which is very close to the results in previous literature (*25*, *29*, *31*).

On the basis of the FFT results of the log-periodic oscillations (Fig. 2D), the frequency peak at $F \approx 2.00$ indicates a period of $\log(B_n) \approx 0.50$ and, naturally, a main scale factor $\lambda = B_n/B_{n+1} \approx 3.16$ for the $ZrTe_5$ system. Considering the FWHM as an error bar, a reasonable λ range [2.30 to 4.00] is deduced for s6 at 4.2 K. The λ range is about [2.38 to 5.80] and [2.4 to 5.30] for s7 and s9, respectively. For channel with $\kappa = 1$, the theoretically estimated factor λ locates in the range of [2.76 to 4.06], and the range becomes broader when considering the contribution from higher angular momentum channels, which is consistent with our experimental observations. On the basis of the model, the amplitude of the oscillations is proportional to the occupation number of the quasi-bound states, which satisfies $N = N_0(1 - \exp(-\Delta E/k_B T))$,

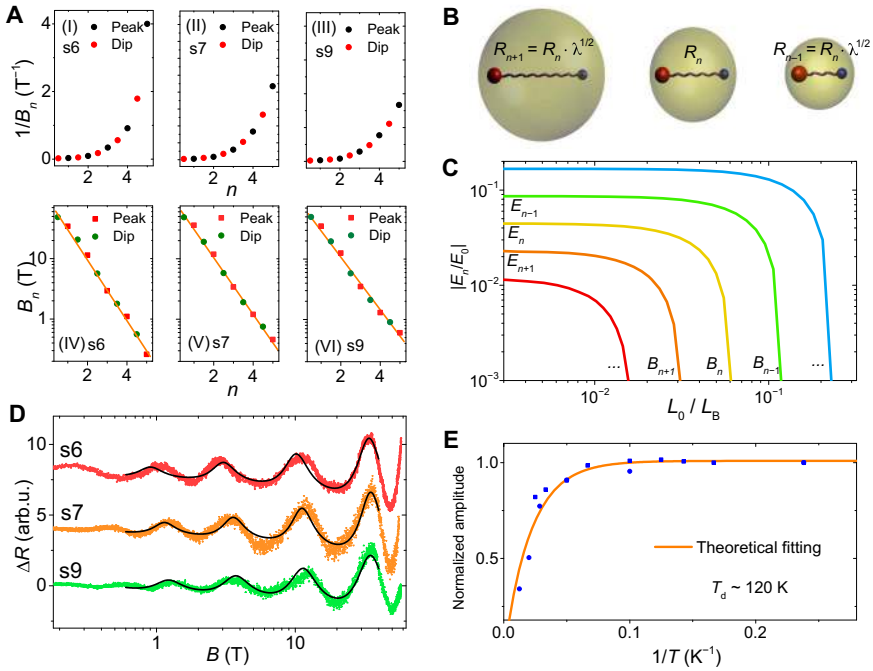

Fig. 4. DSI in ultraquantum $ZrTe_5$. (**A**) Index plot for the log-periodic oscillations. (**B**) Schematic of the two-body quasi-bound states composed of a Dirac-type massless hole and charged center via Coulomb attraction. (**C**) Normalized binding energy of the quasi-bound states under the magnetic field. E_0 and L_0 denote the cutoff scale. (**D**) Quantitative fitting (black curves) of the log-periodic oscillations in $ZrTe_5$. arb.u., arbitrary units. (**E**) Temperature dependence of the normalized amplitude of the oscillation peak $n = 1$. The fitting (orange curve) of the oscillation data (blue points) indicates a disappearance temperature T_d consistent with the experimental results.

where k_B indicates Boltzmann constant. Figure 4E shows the temperature dependence of the oscillatory amplitude of the $n = 1$ peak. The data points (blue points) are from two samples of s6 (circles) and s10 (squares) to show more experimental details. The fitting (orange curve) parameter of the binding energy $\Delta E \sim 10.3$ meV indicates a disappearance temperature $T_d \sim 120$ K, which is also consistent with our experimental results. Thus, the log-periodic MR oscillations can be interpreted by the two-body quasi-bound states scenario. These results would inspire further theoretical investigations to give a clear description of the DSI feature in this many-body system. For example, the screening effect from the continuous band sets a long-range cutoff for the quasi-bound states, and the lattice constant gives the short-range cutoff.

Direct estimation from the carrier density indicates the range with DSI approximately located in the range of 0.4 to 60 nm and, correspondingly, the magnetic field located in the range of 0.2 to 150 T. The continuous band also contributes to the MR, rendering as the envelope of MR data. Moreover, the contribution of higher angular momentum channels to the MR can broaden the approximate DSI range. Typically, a log-log plot is the best way to show the DSI feature in a system. However, in the experimental observations, out of the log-periodic oscillations, other scattering mechanisms also contribute to the measured MR with a nonoscillating background. Thus, background subtraction procedure is necessary to extract the magneto-oscillations, as generally analyzed in condensed matter physics (*16*). The procedure would have influence on the oscillating amplitude, but the process does not affect the periodicity of the oscillations. Thus, the signal of the DSI feature can be detected by the remarkable log periodicity of the MR oscillations, which has been demonstrated in our work by the FFT results (Figs. 2D and 3D) and the index plot with a semilog scale (Fig. 4A). Last, there is certain deviation between the experimental data and fitting curves in the small-field limit and the large-field limit. The reason for this deviation is twofold. First, the boundary condition largely affects the subtracted background at both ending fields. Thus, a small error exists in the characteristic B_n for the oscillations at the boundary magnetic fields due to the influence of subtracted background, which could lead to the deviation of experimental data from the fitting curves. Second, in the large magnetic field limit, the theoretical fitting curves with the consideration of the Zeeman effect can be closer to experimental data. More discussions on the fitting are given in the supplementary materials.

Other physical mechanisms, such as the fractional Hall effect, a Wigner crystal, and a density wave transition, may also exist in a three-dimensional (3D) electronic system beyond the QL (*30*, *38*–*41*). However, the observed oscillations do not agree with the behaviors of these states (see more details in the supplementary materials). For example, the deformation or reconstruction of the Fermi surface by density wave transition commonly occurs at a certain value of magnetic field with the carrier density influenced largely. Then, a remarkable sharp transition can be expected in the MR at the critical magnetic field. However, in our observations, the MR does not show any sharp transition. These mechanisms do not have DSI, while it is a remarkable feature of our experimental results, revealed by the peculiar log periodicity of the five oscillating cycles. The DSI can also exist in a system with fractal property in real space (*1*). However, our samples are high-quality single crystals with no signature of real-space fractal or strong disorder-induced multifractal properties. Therefore, the observed DSI is very likely a notable aspect of the quasi-bound states with geometrical scaling. The three-body model for Efimov states can be excluded, due to the harsh requirement of resonant scattering condition (see

more details in the supplementary materials). Because of the ultralow carrier density in our $ZrTe_5$ samples, the absence of screening effect can give rise to the Coulomb attraction, and the small Fermi velocity in $ZrTe_5$ further guarantees the supercritical collapse condition, which, in combination, result in the two-body quasi-bound states with DSI.

In summary, a new type of quantum oscillations different with previously known $1/B$ periodic SdH effect (*16*) and B periodic AB or AAS effect (*17*) in condensed matter systems has been revealed by our magnetotransport results, which may shed light on the ground state of topological materials beyond the quantum limit. The discovery of the exotic log-periodic oscillations involving five oscillating cycles is a clear manifestation of the rarely observed DSI, which is of high general interest to several fields of physics. Relevant indications for the DSI of the quasi-bound states in solid-state materials may be further detected by other techniques such as the magnetic susceptibilities measurements, thermal transport measurements, and the scanning tunneling spectroscopy. Besides, it will be interesting to extend the present study to a broad range of topological materials (*42*) with Coulomb attraction, as the distinctive log-periodic MR oscillations and the underlying DSI-featured spectrum could be universal.

Note added: After completion of this work, we became aware of a preprint, which addresses the quasi-bound states and the signature of broken continuous scale symmetry in graphene by scanning tunneling microscope (*43*).

MATERIALS AND METHODS

Sample growth

$ZrTe_5$ single crystals used in this work were grown out of Te-flux method. In a typical growth, Zr slug and Te shots in an atomic ratio of 1:49 were loaded into a 2-ml Canfield crucible set (*36*) and then sealed in a silica ampoule under vacuum. The sealed ampoule was heated to 1000°C and kept for 12 hours to homogenize the melt, furnace cooled to 650°C, and then cooled down to 460°C in 60 hours. $ZrTe_5$ crystals were isolated from Te flux by centrifuging at 460°C. Typical $ZrTe_5$ crystals are about 10 to 20 mm long with the other two dimensions in the range of 0.01 to 0.4 mm.

Crystal characterization

The samples were well characterized by measuring x-ray single-crystal diffraction, elemental analysis, electrical resistivity, and thermopower, confirming that our crystals are stoichiometric (*22*). Our energy-dispersive spectroscopy results reveal an atomic ratio of the samples with Zr:Te ≈ 1:5 (table S2). We also used an FEI Titan Cs-corrected cross-sectional STEM operating at 200 kV to further examine the crystalline nature of the $ZrTe_5$ sample.

Transport measurement

Electrical transport measurements in this work were conducted in three measurement systems: a Physics Property Measurement System from Quantum Design for the low temperature and static magnetic field measurements, a pulsed high magnetic field facility at Wuhan National High Magnetic Field Center (China), and a dilution refrigerator MNK126-450 system with static magnetic fields for an ultralow-temperature environment. Results from different systems and different samples are reproducible and consistent. Standard four (six)–probe method was used for measuring resistivity (resistivity and Hall trace) with the excitation current always flowing along the a axis of $ZrTe_5$ in our electrical transport measurements.

Calculation of QL

When all the carriers were confined to the lowest Landau level, the QL is reached. In recent work on $ZrTe_5$ crystals grown via chemical vapor transport using iodine as the transport agent, the carrier density is reported to be 10^{17} to $10^{18}/cm^3$ with an SdH period of 3 to 5 T, which means that the QL can be reached in 3 to 5 T (*23*, *24*). Using Te-flux method, a lower magnetic field (about 1 T) is needed to drive the compound into its QL (*31*). In our growth conditions, the $ZrTe_5$ crystals have the desired stoichiometry and show very low carrier densities (*22*). According to the Onsager relation, our high-quality $ZrTe_5$ samples with the much lower densities should show a smaller SdH period and, simultaneously, the critical field when the system enters the QL is smaller. We usually judged whether a system enters the QL by analyzing its SdH effect. In our samples, it is hard to extract the SdH oscillations that are merged into the sharp increase of MR around 0 T. However, we could estimate the QL magnetic field B_c for our $ZrTe_5$ crystal based on the carrier density. The critical field at which the system enters the QL field can be estimated by the formula (*44*) $B_c = \left(2\pi^4 n^2 \frac{\sqrt{m_a m_c}}{m_b}\right)^{1/3} \left(\frac{\hbar}{e}\right) \approx 3.8 \times 10^{-11} n^{2/3} \left(\frac{\sqrt{m_a m_c}}{m_b}\right)^{1/3}$, where the carrier density is in cm^{-3}, m_a and m_c are masses perpendicular to the magnetic field, and m_b is the mass along the field.

The very low carrier density and the strong anisotropic property (fig. S5) of our bulk $ZrTe_5$ crystals indicate a very small value of the critical field. Assuming the anisotropy of the carrier mass is constant for a specific material, one obtains the critical field $B_c \propto n^{2/3}$. In our calculation, the anisotropic masses for carriers reported in previous literatures are referred. It is estimated that the QL magnetic field for our crystals is about 0.2 T, which is rather small. Thus, the observed oscillations are beyond the QL, which also excludes the SdH effect as the underlying mechanism. Besides, the investigation on the ground state of a 3D electronic gas system beyond the QL is a long-standing research subject (*30*, *38*–*41*). Our work also provides an exciting playground to explore new physics beyond the QL.

Data analysis

Oscillations in the raw MR data are visible, although the MR background is rather large. After subtracting a smooth background for clarity, the MR oscillations become more apparent and are in good agreement with the structures in the original MR data. To be more rigorous, we demonstrated here in detail how we extracted the MR oscillations by different methods in the work to confirm that the oscillations are intrinsic.

In the inset of Fig. 2A, the oscillations were obtained by computing the second derivative for the measured raw data. This is a very convincing and undisputed method, which is usually used to pick up the maximum/minimum. By comparing the oscillations in the derivative result with that in the raw data, we could observe their correspondence and consistency. The oscillations in the static magnetic field measurements show linear dependence for $\log B_n$ versus n (inset of fig. S4F), as shown in the Fig. 4A. The method frequently used to produce a background is doing polynomial fitting, which is used in our work for the creation of fig. S3B. The original raw data are shown in fig. S3A. After subtracting a sixth-order polynomial from the raw data, we obtained the results shown in fig. S3B. The oscillations could be obtained whenever a fifth-/sixth-/seventh-/eighth-order polynomial is subtracted, and we could also observe the correspondence and consistency of the oscillations in fig. S3B with the oscillations on the raw data (fig. S3A).

For the MR in an ultrahigh magnetic field up to 58 T, the whole oscillations could not be shown clearly in the second derivative results due to the large amplitude changes. Meanwhile, a polynomial fitting could not produce a reasonable background curve in the large magnetic field regime. In this case, a smooth background was produced by smoothing the raw data, as shown in fig. S2. The black points are the raw data, and the red line is the produced background. The background at both ends shows tiny anomaly due to unsuitable boundary conditions, and we always discarded the data at the boundaries for further analysis. After subtracting the background from the original data, distinct log-periodic MR oscillations were obtained. The obtained oscillations are also consistent with the oscillations in the raw data and the second derivative results.

In summary, the exotic MR oscillations periodic in logarithmic B are reproducible in different samples, although the data were measured in different systems and analyzed by different methods. The results demonstrate that the oscillations are intrinsic properties of the high-quality $ZrTe_5$ crystals.

SUPPLEMENTARY MATERIALS

Supplementary material for this article is available at http://advances.sciencemag.org/cgi/content/full/4/11/eaau5096/DC1

Table S1. A brief review of the results of $ZrTe_5$.
Table S2. A summary of the energy-dispersive spectroscopy results on our $ZrTe_5$ crystals.
Table S3. Fitting parameters of log-periodic oscillations in different samples.
Table S4. Fitting parameters of log-periodic oscillations in s6 at different temperatures.
Fig. S1. Hall analysis in a two-carrier model.
Fig. S2. Background produced by smoothing the raw MR data.
Fig. S3. Log-periodic MR oscillations in s2 and s10.
Fig. S4. MR oscillations periodic in log$B$ and not in B or 1/B.
Fig. S5. Strong anisotropy of the bulk $ZrTe_5$.
Fig. S6. Theoretical fitting of the experimental results.
Supplementary discussions on other physical mechanisms
Supplementary notes on theoretical details
References (*44*–*57*)

REFERENCES AND NOTES

1. D. Sornette, Discrete-scale invariance and complex dimensions. *Phys. Rep.* **297**, 239–270 (1998).
2. L. D. Landau, E. M. Lifshitz, *Quantum Mechanics: Non-Relativistic Theory* (Perganon Press, ed. 3, 1977).
3. V. Efimov, Energy levels arising from resonant two-body forces in a three-body system. *Phys. Lett. B* **33**, 563–564 (1970).
4. E. Braaten, H. W. Hammer, Universality in few-body systems with large scattering length. *Phys. Rep.* **428**, 259 (2006).
5. P. Naidon, S. Endo, Efimov physics: A review. *Rep. Prog. Phys.* **80**, 056001 (2017).
6. T. Kraemer, M. Mark, P. Waldburger, J. G. Danzl, C. Chin, B. Engeser, A. D. Lange, K. Pilch, A. Jaakkola, H.-C. Nägerl, R. Grimm, Evidence for Efimov quantum states in an ultracold gas of caesium atoms. *Nature* **440**, 315–318 (2006).
7. B. Huang, L. A. Sidorenkov, R. Grimm, J. M. Hutson, Observation of the second triatomic resonance in Efimov's scenario. *Phys. Rev. Lett.* **112**, 190401 (2014).
8. R. Pires, J. Ulmanis, S. Häfner, M. Repp, A. Arias, E. D. Kuhnle, M. Weidemüller, Observation of Efimov resonances in a mixture with extreme mass imbalance. *Phys. Rev. Lett.* **112**, 250404 (2014).
9. S.-K. Tung, K. Jiménez-García, J. Johansen, C. V. Parker, C. Chin, Geometric scaling of Efimov states in a ^{6}Li-^{133}Cs mixture. *Phys. Rev. Lett.* **113**, 240402 (2014).
10. M. Kunitski, S. Zeller, J. Voigtsberger, A. Kalinin, L. P. H. Schmidt, M. Schöffler, A. Czasch, W. Schöllkopf, R. E. Grisenti, T. Jahnke, D. Blume, R. Dörner, Observation of the Efimov state of the helium trimer. *Science* **348**, 551–555 (2015).
11. S. Deng, Z.-Y. Shi, P. Diao, Q. Yu, H. Zhai, R. Qi, H. Wu, Observation of the Efimovian expansion in scale-invariant Fermi gases. *Science* **353**, 371–374 (2016).
12. W. Greiner, B. Muller, J. Rafelski, *Quantum Electrodynamics of Strong Fields* (Springer-Verlag, 1985).
13. A. V. Shytov, M. I. Katsnelson, L. S. Levitov, Atomic collapse and quasi–Rydberg states in graphene. *Phys. Rev. Lett.* **99**, 246802 (2007).
14. Y. Nishida, Vacuum polarization of graphene with a supercritical Coulomb impurity: Low-energy universality and discrete scale invariance. *Phys. Rev. B* **90**, 165414 (2014).
15. L. Schubnikow, W. J. de Haas, A new phenomenon in the change of resistance in a magnetic field of single crystals of bismuth. *Nature* **126**, 500 (1930).
16. D. Schoenberg, *Magnetic Oscillations in Metals* (Cambridge Univ. Press, 1984).
17. Y. Imry, *Introduction to Mesoscopic Physics* (Oxford Univ. Press, 1997).
18. S. Okada, T. Sambongi, M. Ido, Giant resistivity anomaly in $ZrTe_5$. *J. Phys. Soc. Jpn.* **49**, 839–840 (1980).
19. T. M. Tritt, N. D. Lowhorn, R. T. Littleton IV, A. Pope, C. R. Feger, J. W. Kolis, Large enhancement of the resistive anomaly in the pentatelluride materials $HfTe_5$ and $ZrTe_5$ with applied magnetic field. *Phys. Rev. B* **60**, 7816–7819 (1999).
20. G. N. Kamm, D. J. Gillespie, A. C. Ehrlich, T. J. Wieting, F. Levy, Fermi surface, effective masses, and Dingle temperatures of $ZrTe_5$ as derived from the Shubnikov–de Haas effect. *Phys. Rev. B* **31**, 7617–7623 (1985).
21. H. Weng, X. Dai, Z. Fang, Transition-metal pentatelluride $ZrTe_5$ and $HfTe_5$: A paradigm for large-gap quantum spin Hall insulators. *Phys. Rev. X* **4**, 011002 (2014).
22. P. Shahi, D. J. Singh, J. P. Sun, L. X. Zhao, G. F. Chen, J.-Q. Yan, D. G. Mandrus, J.-G. Cheng, Bipolar conduction is the origin of the electronic transition in pentatellurides: Metallic vs semiconducting behavior. *Phys. Rev. X* **8**, 021055 (2018).
23. Y. Liu, X. Yuan, C. Zhang, Z. Jin, A. Narayan, C. Luo, Z. Chen, L. Yang, J. Zou, X. Wu, S. Sanvito, Z. Xia, L. Li, Z. Wang, F. Xiu, Zeeman splitting and dynamical mass generation in Dirac semimetal $ZrTe_5$. *Nat. Commun.* **7**, 12516 (2016).
24. G. Zheng, J. Lu, X. Zhu, W. Ning, Y. Han, H. Zhang, J. Zhang, C. Xi, J. Yang, H. Du, K. Yang, Y. Zhang, M. Tian, Transport evidence for the three-dimensional Dirac semimetal phase in $ZrTe_5$. *Phys. Rev. B* **93**, 115414 (2016).
25. Q. Li, D. E. Kharzeev, C. Zhang, Y. Huang, I. Pletikosić, A. V. Fedorov, R. D. Zhong, J. A. Schneeloch, G. D. Gu, T. Valla, Chiral magnetic effect in $ZrTe_5$. *Nat. Phys.* **12**, 550–554 (2016).
26. D. N. McIlroy, S. Moore, D. Zhang, J. Wharton, B. Kempton, R. Littleton, M. Wilson, T. M. Tritt, C. G. Olson, Observation of a semimetal semiconductor phase transition in the intermetallic $ZrTe_5$. *J. Phys. Condens. Matter* **16**, L359–L365 (2004).
27. Y.-Y. Lv, F. Zhang, B.-B. Zhang, B. Pang, S.-H. Yao, Y. B. Chen, L. Ye, J. Zhou, S.-T. Zhang, Y.-F. Chen, Microstructure, growth mechanism and anisotropic resistivity of quasi-one-dimensional $ZrTe_5$ crystal. *J. Cryst. Growth* **457**, 250–254 (2017).
28. Z. Fan, Q.-F. Liang, Y. B. Chen, S.-H. Yao, J. Zhou, Transition between strong and weak topological insulator in $ZrTe_5$ and $HfTe_5$. *Sci. Rep.* **7**, 45667 (2017).
29. H. Chi, C. Zhang, G. Gu, D. E. Kharzeev, X. Dai, Q. Li, Lifshitz transition mediated electronic transport anomaly in bulk $ZrTe_5$. *New J. Phys.* **19**, 015005 (2017).
30. W. Yu, Y. Jiang, J. Yang, Z. L. Dun, H. D. Zhou, Z. Jiang, P. Lu, W. Pan, Quantum oscillations at integer and fractional Landau level indices in single-crystalline $ZrTe_5$. *Sci. Rep.* **6**, 35357 (2016).
31. R. Y. Chen, Z. G. Chen, X.-Y. Song, J. A. Schneeloch, G. D. Gu, F. Wang, N. L. Wang, Magnetoinfrared spectroscopy of Landau levels and Zeeman splitting of three-dimensional massless Dirac fermions in $ZrTe_5$. *Phys. Rev. Lett.* **115**, 176404 (2015).
32. T. Liang, J. Lin, Q. Gibson, S. Kushwaha, M. Liu, W. Wang, H. Xiong, J. A. Sobota, M. Hashimoto, P. S. Kirchmann, Z.-X. Shen, R. J. Cava, N. P. Ong, Anomalous Hall effect in $ZrTe_5$. *Nat. Phys.* **14**, 451–455 (2018).
33. G. Zheng, X. Zhu, Y. Liu, J. Lu, W. Ning, H. Zhang, W. Gao, Y. Han, J. Yang, H. Du, K. Yang, Y. Zhang, M. Tian, Field-induced topological phase transition from a three-dimensional Weyl semimetal to a two-dimensional massive Dirac metal in $ZrTe_5$. *Phys. Rev. B* **96**, 121401 (2017).
34. J. Niu, J. Wang, Z. He, C. Zhang, X. Li, T. Cai, X. Ma, S. Jia, D. Yu, X. Wu, Electrical transport in nanothick $ZrTe_5$ sheets: From three to two dimensions. *Phys. Rev. B* **95**, 035420 (2017).
35. Y. Jiang, Z. L. Dun, H. D. Zhou, Z. Lu, K.-W. Chen, S. Moon, T. Besara, T. M. Siegrist, R. E. Baumbach, D. Smirnov, Z. Jiang, Landau-level spectroscopy of massive Dirac fermions in single-crystalline $ZrTe_5$ thin flakes. *Phys. Rev. B* **96**, 041101 (2017).
36. P. C. Canfield, T. Kong, U. S. Kaluarachchi, N. H. Jo, Use of frit-disc crucibles for routine and exploratory solution growth of single crystalline samples. *Philos. Mag.* **96**, 84 (2016).
37. R. A. Smith, *Semiconductors* (Cambridge Univ. Press, 1978).
38. B. I. Halperin, Possible states for a three-dimensional electron gas in a strong magnetic field. *Jpn. J. Appl. Phys.* **26**, 1913–1919 (1987).
39. K. Behnia, L. Balicas, Y. Kopelevich, Signatures of electron fractionalization in ultraquantum bismuth. *Science* **317**, 1729–1731 (2007).
40. J. G. Analytis, R. D. McDonald, S. C. Riggs, J.-H. Chu, G. S. Boebinger, I. R. Fisher, Two-dimensional surface state in the quantum limit of a topological insulator. *Nat. Phys.* **6**, 960–964 (2010).
41. L. Li, J. G. Checkelsky, Y. S. Hor, C. Uher, A. F. Hebard, R. J. Cava, N. P. Ong, Phase transitions of Dirac electrons in bismuth. *Science* **321**, 547–550 (2008).
42. H. Weng, X. Dai, Z. Fang, Topological semimetals predicted from first-principles calculations. *J. Phys. Condens. Matter* **28**, 303001 (2016).
43. O. Ovdat, J. Mao, Y. Jiang, E. Y. Andrei, E. Akkermans, Observing a scale anomaly and a universal quantum phase transition in graphene. *Nat. Commun.* **8**, 507 (2017).
44. H. Li, H. He, H.-Z. Lu, H. Zhang, H. Liu, R. Ma, Z. Fan, S.-Q. Shen, J. Wang, Negative magnetoresistance in Dirac semimetal Cd_3As_2. *Nat. Commun.* **7**, 10301 (2016).

45. D. G. Seiler, A. E. Stephens, The Shubnikov–de Haas effect in semiconductors: A comprehensive review of experimental aspects, in *Landau Level Spectroscopy*, G. Landwehr, E. I. Rashba, Eds. (Elsevier Science Publishers, 1991).
46. J. Cao, S. Liang, C. Zhang, Y. Liu, J. Huang, Z. Jin, Z.-G. Chen, Z. Wang, Q. Wang, J. Zhao, S. Li, X. Dai, J. Zou, Z. Xia, L. Li, F. Xiu, Landau level splitting in Cd_3As_2 under high magnetic fields. *Nat. Commun.* **6**, 7779 (2015).
47. X. Huang, L. Zhao, Y. Long, P. Wang, D. Chen, Z. Yang, H. Liang, M. Xue, H. Weng, Z. Fang, X. Dai, G. Chen, Observation of the chiral-anomaly-induced negative magnetoresistance in 3D Weyl semimetal TaAs. *Phys. Rev. X* **5**, 031023 (2015).
48. P. L. Cai, J. Hu, L. P. He, J. Pan, X. C. Hong, Z. Zhang, J. Zhang, J. Wei, Z. Q. Mao, S. Y. Li, Drastic pressure effect on the extremely large magnetoresistance in WTe_2: Quantum oscillation study. *Phys. Rev. Lett.* **115**, 057202 (2015).
49. Y. Zhao, H. Liu, C. Zhang, H. Wang, J. Wang, Z. Lin, Y. Xing, H. Lu, J. Liu, Y. Wang, S. M. Brombosz, Z. Xiao, S. Jia, X. C. Xie, J. Wang, Anisotropic Fermi surface and quantum limit transport in high mobility three-dimensional Dirac semimetal Cd_3As_2. *Phys. Rev. X* **5**, 031037 (2015).
50. D. C. Tsui, H. L. Stormer, A. C. Gossard, Two-dimensional magnetotransport in the extreme quantum limit. *Phys. Rev. Lett.* **48**, 1559–1562 (1982).
51. Y. Kopelevich, B. Raquet, M. Goiran, W. Escoffier, R. R. da Silva, J. C. Medina Pantoja, I. A. Luk'yanchuk, A. Sinchenko, P. Monceau, Searching for the fractional quantum Hall effect in graphite. *Phys. Rev. Lett.* **103**, 116802 (2009).
52. B. Fauqué, D. LeBoeuf, B. Vignolle, M. Nardone, C. Proust, K. Behnia, Two phase transitions induced by a magnetic field in graphite. *Phys. Rev. Lett.* **110**, 266601 (2013).
53. C.-L. Zhang, B. Tong, Z. Yuan, Z. Lin, J. Wang, J. Zhang, C.-Y. Xi, Z. Wang, S. Jia, C. Zhang, Signature of chiral fermion instability in the Weyl semimetal TaAs above the quantum limit. *Phys. Rev. B* **94**, 205120 (2016).
54. J. J. Sakurai, J. J. Napolitano, *Modern Quantum Mechanics* (Pearson Higher Ed., 2014).
55. C. M. Bender, S. A. Orszag, *Advanced Mathematical Methods for Scientists and Engineers I: Asymptotic Methods and Perturbation Theory* (Springer-Verlag, 1999).
56. H. Liu, H. Jiang, Z. Wang, R. Joynt, X. C. Xie, Discrete scale invariance in topological semimetals. arXiv:1807.02459 [cond-mat.mtrl-sci] (6 July 2018).
57. A. A. Abrikosov, Quantum magnetoresistance. *Phys. Rev. B* **58**, 2788–2794 (1998).

Acknowledgments: We acknowledge Y. Liu, J. Cheng, X. Lin, R. Zhang, and Z. Lin for the help in related experiments and H. Lu, F. Wang, and Q. Zhu for valuable discussions. **Funding:** This work was financially supported by the National Basic Research Program of China (grant nos. 2018YFA0305604, 2013CB934600, 2017YFA0303300, and 2015CB921102), the Research Fund for the Doctoral Program of Higher Education of China (grant no. 20130001110003), the National Natural Science Foundation of China (grants nos. 11774008, 11534001, 11674028, 11504008, 51390474, and 11234011), the Open Project Program of the Pulsed High Magnetic Field Facility (grant no. PHMFF2015002) at the Huazhong University of Science and Technology, and the Strategic Priority Research Program of Chinese Academy of Sciences (grant no. XDB28000000). J.Y. is supported by the U.S. Department of Energy, Office of Science, Basic Energy Sciences, Materials Sciences and Engineering Division. D.M. was supported by the Gordon and Betty Moore Foundation's EPiQS Initiative through grant no. GBMF4416. H.W. acknowledges the Postdoctoral Fellowships Scheme of the Hong Kong Polytechnic University (project no. 1-YW0T).

Author contributions: Jian Wang conceived and instructed the experiments. H.W. performed the experiments and analyzed the experimental results. H.L. and X.C.X. proposed and developed the theoretical model. J.Y. and D.M. synthesized the samples. Y. Li, Y. Liu, Junfeng Wang, L.L., and J.-Y.D. helped in the transport measurements. J.L. and Y.W. performed the transmission electron microscopy characterization. H.W., H.L., and Jian Wang wrote the paper with the assistance of X.C.X. and contribution of J.Y. and D.M. **Competing interests:** The authors declare that they have no competing interests. **Data and materials availability:** All data needed to evaluate the conclusions in the paper are present in the paper and/or the Supplementary Materials. Additional data related to this paper may be requested from the authors.

Submitted 18 June 2018
Accepted 25 September 2018
Published 2 November 2018
10.1126/sciadv.aau5096

Citation: H. Wang, H. Liu, Y. Li, Y. Liu, J. Wang, J. Liu, J.-Y. Dai, Y. Wang, L. Li, J. Yan, D. Mandrus, X. C. Xie, J. Wang, Discovery of log-periodic oscillations in ultraquantum topological materials. *Sci. Adv.* **4**, eaau5096 (2018).

Discovery of log-periodic oscillations in ultraquantum topological materials

Huichao Wang, Haiwen Liu, Yanan Li, Yongjie Liu, Junfeng Wang, Jun Liu, Ji-Yan Dai, Yong Wang, Liang Li, Jiaqiang Yan, David Mandrus, X. C. Xie and Jian Wang

Sci Adv **4** (11), eaau5096.
DOI: 10.1126/sciadv.aau5096